Mechanical Systems and Signal Processing 39 (2013) 227–244

Contents lists available at SciVerse ScienceDirect

Mechanical Systems and Signal Processing

journal homepage: www.elsevier.com/locate/ymssp

Identification of dynamic stiffness matrices of elastomeric joints using direct and inverse methods

Scott Noll, Jason T. Dreyer, Rajendra Singh *

Acoustics and Dynamics Laboratory, Smart Vehicle Concepts Center, Department of Mechanical and Aerospace Engineering, The Ohio State University, Columbus, OH 43210, USA

ARTICLE INFO

Article history:
Received 24 August 2012
Received in revised form
18 January 2013
Accepted 3 February 2013
Available online 13 March 2013

Keywords:
Joint identification
Experimental dynamics
Stiffness coupling
Elastomer properties
Beam structures

ABSTRACT

New experiments are designed to permit direct comparison between direct and inverse identification methods of the dynamic stiffness matrices of elastomeric joints, including non-diagonal terms. The joints are constructed with combinations of inclined elastomeric cylinders to control non-diagonal terms in the stiffness matrix. The inverse experiment consists of an elastic metal beam end-supported by elastomeric joints coupling the in-plane transverse and longitudinal beam motion. A prior method is extended to identify the joint dynamic stiffness matrices of dimension 3 from limited modal measurements of the beam. The dynamic stiffness and loss factors of the elastomeric cylinders are directly measured in a commercial elastomer test machine in shear, compression, and inclined configurations and a coordinate transformation is used to estimate the kinematic non-diagonal stiffness terms. Agreement is found for both dynamic stiffness and loss factors between the direct and inverse methods at small displacements. Further, the identified joint properties are employed in a model that successfully predicts the modal parameters and accelerance spectra of the inverse experiment. This article provides valuable insight on the difficulties encountered when comparing system and elastomeric component test results.

1. Introduction

Joints such as fasteners, welds, bearings, and elastomers present many challenges in modeling, and thus, the development of identification methods has drawn much attention [1–11]. Overall, the knowledge of joint parameters is often limited to a single stiffness or damping term [1–7,8]. In some experimental studies, the accuracy of the identified results are evaluated by means of deduction only [5,6,9], assuming that the response of the assembly must be accurately predicted from substructure models or frequency response functions and the identified joint parameters. In particular, elastomeric joints are widely used in vehicle isolation systems and their geometries are shaped to provide favorable properties in certain directions based on the diagonal terms [12]. Nonetheless, non-diagonal (coupling) terms are often unknown though they are intrinsic to the design of complex automotive assemblies [13]. Joint models in experimental identification studies have been limited to either a single joint stiffness term [3,4,7,8] or elastic coupling between transverse deflection and slope of dimension 2 [1,2,5,6,9–11]. Measurement of the multidimensional dynamic properties of practical elastomeric joints with complicated shapes is a difficult task, and these properties are further complicated

* Corresponding author: Tel.: +1 614 292 9044.
E-mail address: singh.3@osu.edu (R. Singh).

0888-3270/$ - see front matter © 2013 Elsevier Ltd. All rights reserved.
http://dx.doi.org/10.1016/j.ymssp.2013.02.003

when an elastomeric component is integrated into a sub-system assembly. Typically, the dynamic properties of assemblies may differ from those of components due to preload and boundary condition effects. Therefore, there is a need to develop improved experimental methods to examine these issues [14].

Identification methods that utilize computational and experimental modal analyses may be integrated into some applications as long as the structures behave in a linear manner [15,16]. For instance, Kim et al. [3] used a modal-based technique to characterize the dynamic stiffness of beam supports, each modeled by a lumped transverse spring. This method used the physical system matrices developed from a discretized model (lumped parameter or finite element) without joints, and then measured eigenvalues and eigenvectors are utilized to extract the joint parameters. Their formulation explicitly assumed that the joints did not contain any coupling terms, and the experimental validation considered only a single stiffness term without damping. To overcome the above-mentioned limitations, this article proposes new or improved direct and inverse experiments which will yield the elastomeric joint dynamic stiffness matrices, including non-diagonal terms. Additionally, the prior formulation of Kim et al. [3] will be extended to permit identification of the coupled damping and stiffness matrices in the inverse experiment.

2. Problem formulation

The conceptual problem formulation is illustrated in Fig. 1 where a beam is supported on multidimensional joints at each end. Kinematic coupling to the structure is introduced through inclined attachment of the joints which couples the transverse $y(x,t)$ and longitudinal $u(x,t)$ motions of the beam. Based on representative real-world automotive elastomeric joints and subframe structures, the joint stiffness aspect ratio, R, is selected at a nominal value of 7 and the modal parameters of the unconstrained (free–free) beam are selected with the first elastic flexural mode between 100 and 200 Hz. Further, the first 3 rigid body and 3 elastic modes (up to 1024 Hz) are examined, as both rigid and elastic modes are of concern in practical assemblies. Elastomeric joints are intentionally selected even though they exhibit excitation amplitude and frequency dependent properties, as well as sample to sample variations. Given the amplitude-dependent properties, comparisons must be made with a direct method. Both inverse and direct methods are employed in industry, from system and component perspectives, respectively.

The scope of the inverse test is limited to an elastic beam structure connected to ground through two elastomeric joints, where each joint is comprised of two cylinders. The assembled system is assumed to be linear time invariant and self-adjoint; the damping of the elastomeric joints is structural, and the beam is assumed to be proportionally viscous damped. Further, the joint mass is known *a priori*, and the dynamic properties of a joint can be represented at a point by structural damping **h** and stiffness **k** matrices. The specific objectives of this article are as follows:

- Design a tractable inverse beam experiment that allows a comparison with the direct test of an elastomeric component.
- Extend the prior inverse formulation of Kim et al. [3] to include identification of fully populated joint dynamic matrices given limited modal measurements from the inverse beam experiment.

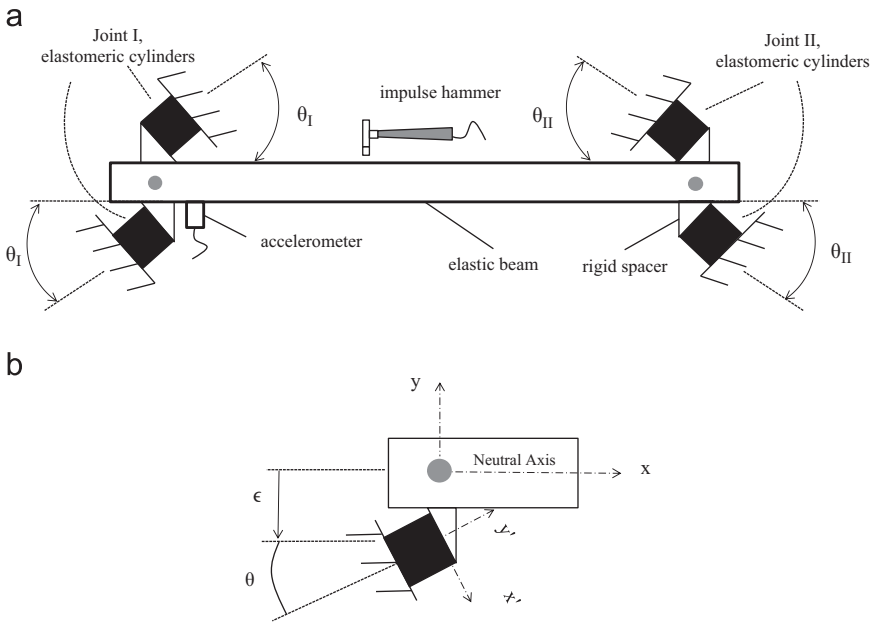

Fig. 1. Conceptual formulation of the resonant test: (a) elastic beam is end supported by two joints, where each joint is comprised of two inclined elastomeric cylinders and (b) details of transverse eccentricity, ε, and angle of inclination, θ.

- Computationally examine uniqueness and conditioning of the proposed inverse method with respect to the beam experiment.
- Conduct validation experiments on a beam supported by two elastomeric joints.

The proposed objectives permit a comparison between the dynamic joint properties identified with inverse and direct test methods; having consistency between the two different methods would suggest a heuristic validation though these two methods are rarely compared in the scientific literature.

3. Inverse beam experiment with two elastomeric joints

A rigid body formulation alone will not permit a sufficient number of equations to uniquely identify the two different joints in the inverse beam experiment; thus an elastic body formulation is required. Further, the elastomeric cylinders are selected to have similar (but non-identical) stiffness properties to automotive bushings and ratio of joint to structure stiffness. To maintain the lumped joint stiffness assumption, the ratio of the contact surface dimension to beam length is kept below 0.05. With these guidelines, a steel beam (with Young's modulus, $E = 207$ GPa, Poisson's ratio, $\nu = 0.3$, and mass density, $\rho = 7850\ \mathrm{kg\ m^{-3}}$) is selected. The beam is 914 mm in length (L), the rectangular cross-sectional area (A) is 1290 $\mathrm{mm^2}$, and the transverse height is 25.4 mm. Modal measurements are made on the beam while it is suspended by very compliant springs. Since the frequency range of interest (up to 1024 Hz) is well below that of the first elastic longitudinal natural frequency, only $y(x,t)$ responses are collected though the dynamic force is applied in both directions.

The beam is supported near each end by a combination of two angled elastomeric cylinders, specified as Neoprene with a Shore A hardness of 70. To introduce coupling, yet maintain the self-adjoint assumption, angled cylinders with an aspect ratio of 7 are inclined at 45° from above and below the beam. The angled cylinders induce local coupling between the transverse and longitudinal movements of the beam at the joint. The formulation in the next section demonstrates the intended symmetry of the joint stiffness matrix.

A modal experiment is conducted for the inverse beam experiment as depicted in Fig. 1. The accelerometer is positioned below point 3 (corresponds to node 3 of Fig. 2), and the roving impulse hammer technique is employed, with force inputs at points 1, 3–9, and 11 in the transverse direction and at points 1 and 11 in the longitudinal direction; note that impacts directly at the joint location are not possible. Ten impacts at each location are averaged to minimize random error in the accelerance $\tilde{A}_{ij}(\omega)$ measurements. For this work, a polyreference least-squares complex frequency-domain method is utilized where this implementation estimates the natural frequencies, damping parameters, and eigenvectors in a global sense [16].

Although this measurement set results in eigenvector estimates at each location, only the results near the joint locations are utilized in the identification procedure, e.g. at joint I, the eigenvector components at points 1 and 3 are used. These points permit the best interpolation of the eigenvector components at point 2 (joint I) for transverse and slope degrees of freedom since they could not be directly measured. (The interpolation method is described later in Section 5.)

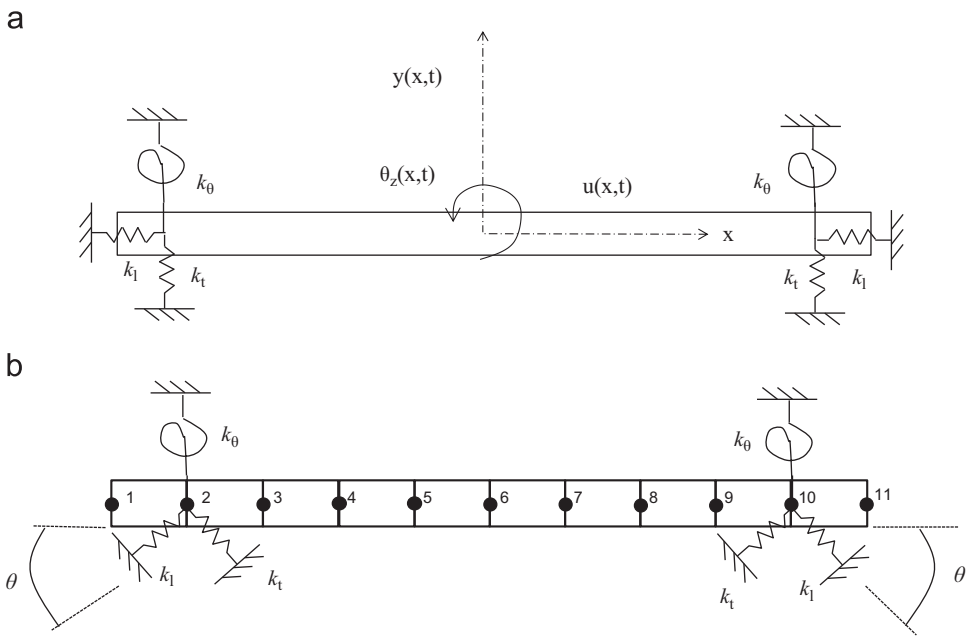

Fig. 2. Problem formulation (a) diagonal support stiffnesses of an elastic beam (b) computational beam model with 10 elements and 11 nodes with kinematic coupling introduced through support inclination. Lumped stiffness elements are attached at nodes 2 and 10.

Since the frequency range of interest is well below the longitudinal elastic modes, the two measured eigenvector components in the longitudinal direction at points 1 and 11 are averaged in magnitude and phase. This aids in correcting some experimental measurement errors prior to use in the identification procedure. After identification, the joint dynamic stiffness matrices are employed with the beam model to forward predict the eigensolutions and frequency response functions of the experiment.

4. Analytical model of inverse beam test

4.1. Computational model of beam using aTimoshenko formulation

The computational model is comprised of 10 beam finite elements with lumped dynamic stiffness matrices at nodes 2 and 10 as depicted in Fig. 2. A two-node Timoshenko beam element is superposed with a longitudinal rod element to generate a two-node six degree of freedom element. This formulation assumes that elastic longitudinal and beam bending are uncoupled. The work of Friedman and Kosmatka [17] contains a complete derivation of the finite element stiffness and mass matrices for a Timoshenko beam. The stiffness matrix for longitudinal degrees of freedom is written as

$$\mathbf{K}_l = \frac{EA}{L_e}\begin{bmatrix} 1 & -1 \\ -1 & 1 \end{bmatrix}, \tag{1}$$

where L_e is the element length. The corresponding mass matrix for longitudinal motion is

$$\mathbf{M}_l = \frac{\rho A L_e}{6}\begin{bmatrix} 2 & 1 \\ 1 & 2 \end{bmatrix}. \tag{2}$$

The stiffness matrix for the Timoshenko beam is

$$\mathbf{K}_b = \frac{EI}{(1+\phi)L_e^3}\begin{bmatrix} 12 & 6L_e & -12 & 6L_e \\ 6L_e & (4+\phi)L_e^2 & -6L_e & (2-\phi)L_e^2 \\ -12 & -6L & 12 & -6L_e \\ 6L_e & (2-\phi)L_e^2 & -6L_e & (4+\phi)L_e^2 \end{bmatrix}, \tag{3}$$

where I is the area moment of inertia, and ϕ is the ratio of the beam bending stiffness to the shear stiffness given by

$$\phi = \frac{12}{L_e^2}\left(\frac{EI}{\kappa GA}\right) = \frac{24}{L_e^2}\left(\frac{I}{\kappa A}\right)(1+\nu), \tag{4}$$

where G is the shear modulus, and κ is the shear correction factor, and is given for the rectangular cross-section as

$$\kappa = \frac{10(1+\nu)}{12+11\nu}. \tag{5}$$

The consistent mass matrix for the Timoshenko element is comprised of two parts, $\mathbf{M}_b = \mathbf{M}_{bT} + \mathbf{M}_{bR}$, where

$$\mathbf{M}_{bT} = \frac{\rho A L_e}{210(1+\phi)^2}\begin{bmatrix} (70\phi^2+147\phi+78) & (35\phi^2+77\phi+44)\frac{L_e}{4} & (35\phi^2+63\phi+27) & -(35\phi^2+63\phi+26)\frac{L_e}{4} \\ & (7\phi^2+14\phi+8)\frac{L_e^2}{4} & (35\phi^2+63\phi+26)\frac{L_e}{4} & -(7\phi^2+14\phi+6)\frac{L_e^2}{4} \\ & & (70\phi^2+147\phi+78) & -(35\phi^2+77\phi+44)\frac{L_e}{4} \\ \textit{symmetric} & & & (7\phi^2+14\phi+8)\frac{L_e^2}{4} \end{bmatrix} \tag{6}$$

is associated with the translational inertia and

$$\mathbf{M}_{bR} = \frac{\rho I}{30(1+\phi)^2 L_e}\begin{bmatrix} 36 & -(15\phi-3)L_e & -36 & -(15\phi-3)L_e \\ & (10\phi^2+5\phi+4)L_e^2 & (15\phi-3)L_e & (5\phi^2-5\phi-1)L_e^2 \\ & & 36 & (15\phi-3)L_e \\ \textit{symmetric} & & & (10\phi^2+5\phi+4)L_e^2 \end{bmatrix} \tag{7}$$

is associated with the rotary inertia.

The mass matrix reduces to the consistent translational and rotary inertia mass matrices for the Bernoulli–Euler beam theory by setting $\phi = 0$. Similarly, the stiffness matrix reduces the stiffness to that associated with bending only, with infinite shear stiffness.

4.2. Joint stiffness matrix formulation

Each elastomeric cylinder in the inverse experiment has a transverse eccentricity ε from the neutral axis of the beam and an inclination angle θ from the beam's nodal coordinate system as shown in Fig. 1b. Both the eccentricity and the inclination angle introduce a form of kinematic coupling that must be considered such that a suitable transformation can be made from the local coordinate system of the cylinder to the beam's nodal coordinate system. A uniform circular

cylinder when grounded at one end exhibits a stiffness matrix in a local coordinate system as

$$\mathbf{k}_{cyl} = \begin{bmatrix} a & 0 & d \\ 0 & b & 0 \\ d & 0 & c \end{bmatrix}, \tag{8}$$

where a is the shear stiffness, b is the compressive stiffness, c is the rotational stiffness, and d is the elastic coupling between rotation and shear. Assuming that the point stiffness at the end of the cylinder follows a rigid connection to the beam node, the effective stiffness matrix of the elastomeric cylinder in the beam nodal coordinate system can be computed by

$$\mathbf{k}_{eff} = \mathbf{T}_{\varepsilon}\mathbf{T}_{\theta}^{-1}\mathbf{k}\mathbf{T}_{\theta}\mathbf{T}_{\varepsilon}^{\mathrm{T}}, \tag{9}$$

where $\mathbf{T}_{\theta}$ and $\mathbf{T}_{\varepsilon}$ are defined as

$$\mathbf{T}_{\theta} = \begin{bmatrix} \cos\theta & \sin\theta & 0 \\ -\sin\theta & \cos\theta & 0 \\ 0 & 0 & 1 \end{bmatrix} \text{ and } \mathbf{T}_{\varepsilon} = \begin{bmatrix} 1 & 0 & 0 \\ 0 & 1 & 0 \\ -\varepsilon & 0 & 1 \end{bmatrix}. \tag{10a-b}$$

To illustrate this procedure, consider the joint comprised of two cylinders at the left hand of the inverse beam test. The cylinder below the beam is inclined at a positive 45° and has an eccentricity of negative ε; whereas the cylinder above is inclined at negative 135° and has an eccentricity of positive ε. The effective stiffness is thus the superposition of both cylinder point stiffnesses transformed to the beam node as

$$\begin{aligned} \mathbf{k}_{eff} &= \frac{1}{2}\begin{bmatrix} (a+b) & (a-b) & \varepsilon(a+b)+\sqrt{2}d \\ (a-b) & (a+b) & \varepsilon(a-b)+\sqrt{2}d \\ \varepsilon(a+b)+\sqrt{2}d & \varepsilon(a-b)+\sqrt{2}d & 2c+2\sqrt{2}\varepsilon d+\varepsilon^2(a+b) \end{bmatrix} \\ &\quad +\ldots\frac{1}{2}\begin{bmatrix} (a+b) & (a-b) & -\varepsilon(a+b)-\sqrt{2}d \\ (a-b) & (a+b) & -\varepsilon(v)-\sqrt{2}d \\ -\varepsilon(a+b)-\sqrt{2}d & -\varepsilon(a-b)-\sqrt{2}d & 2c+2\sqrt{2}\varepsilon d+\varepsilon^2(a+b) \end{bmatrix} \\ &= \begin{bmatrix} a+b & a-b & 0 \\ a-b & a+b & 0 \\ 0 & 0 & 2c+2\sqrt{2}\varepsilon d+\varepsilon^2(a+b) \end{bmatrix}. \end{aligned} \tag{11}$$

A simpler, yet equivalent, model is the system model of a continuous beam represented by the finite element method with lumped supports at nodes 2 and 10. The support stiffness contains only diagonal elements (Fig. 2a) as

$$\mathbf{k}_j = \begin{bmatrix} k_l & 0 & 0 \\ 0 & k_t & 0 \\ 0 & 0 & k_\theta \end{bmatrix} = \overline{k}\frac{EI}{2L^3}\begin{bmatrix} R & 0 & 0 \\ 0 & 1 & 0 \\ 0 & 0 & \overline{k}_\theta L^2 \end{bmatrix}, \tag{12}$$

where the aspect ratio is defined as $R = k_l/k_t$, the non-dimensional scaling parameter is $\overline{k} = k_t L^3/EI$, and the non-dimensional rotational stiffness parameter is $\overline{k}_\theta = k_\theta/k_t L^2$. The terms of the joint stiffness matrices are normalized by the following stiffness values associated with the structure for rotational stiffness (EI/L), coupling stiffness between a translational and rotational degrees of freedom (EI/L^2), and translation stiffness (EI/L^3). The kinematic coupling terms, k_{12} and k_{21}, between the longitudinal and transverse directions are introduced by inclining the supports (Fig. 2b) to a specified angle, θ, computed by

$$k_{11} = R\cos^2(\theta)+\sin^2(\theta), \tag{13}$$

$$k_{22} = R\sin^2(\theta)+\cos^2(\theta), \tag{14}$$

$$k_{21} = k_{12} = (R-1)\sin(\theta)\cos(\theta). \tag{15}$$

When $R=1$, no kinematic coupling is introduced, i.e. $k_{21}=k_{12}=0$. Assuming that the two end supports are diametrically opposed by an inward rotation of $\theta=45°$, then the joint stiffness matrix is written as

$$\mathbf{k}_{\mathrm{I}} = \overline{k}\frac{EI}{2L^3}\begin{bmatrix} R+1 & R-1 & 0 \\ R-1 & R+1 & 0 \\ 0 & 0 & \overline{k}_\theta L^2 \end{bmatrix} \text{ and } \mathbf{k}_{\mathrm{II}} = \overline{k}\frac{EI}{2L^3}\begin{bmatrix} R+1 & -R+1 & 0 \\ -R+1 & R+1 & 0 \\ 0 & 0 & \overline{k}_\theta L^2 \end{bmatrix}. \tag{16a-b}$$

Note that the coupling elements for joint II (at the other end) exhibit negative values imposed by the kinematics.

5. Development of joint identification method for the inverse beam experiment

The equations of motion for a discrete structure of with N degrees of freedom at the rth mode is as follows where λ_r is the eigenvalue, and ψ_r is the eigenvector (both complex valued)

$$\{\lambda_r^2\mathbf{M}+\lambda_r\mathbf{C}+\mathbf{K}+\mathbf{k}+i\mathbf{h}\}\,\boldsymbol{\psi}_r=\mathbf{0}, \tag{17}$$

where **M**, **C**, and **K** are the mass, viscous damping, and stiffness matrices of the unconstrained structure (without any joints) respectively. Since a steel structure is virtually undamped, **C** can be neglected or computed assuming proportional damping [3]. The joint stiffness matrix **k** and structural damping matrix **h** are sparse with a total of α sub-matrices, defined as $\mathbf{k}_j$ and $\mathbf{h}_j$, associated with the jth joint

$$\mathbf{k}=\begin{bmatrix}\mathbf{k}_1 & \mathbf{0} & \mathbf{0} & \mathbf{0} & \mathbf{0}\\ \mathbf{0} & \mathbf{0} & \mathbf{0} & \mathbf{0} & \mathbf{0}\\ \mathbf{0} & \mathbf{0} & \mathbf{k}_j & \mathbf{0} & \mathbf{0}\\ \mathbf{0} & \mathbf{0} & \mathbf{0} & \ddots & \vdots\\ \mathbf{0} & \mathbf{0} & \mathbf{0} & \dots & \mathbf{k}_\alpha\end{bmatrix} \text{ and } \mathbf{h}=\begin{bmatrix}\mathbf{h}_1 & \mathbf{0} & \mathbf{0} & \mathbf{0} & \mathbf{0}\\ \mathbf{0} & \mathbf{0} & \mathbf{0} & \mathbf{0} & \mathbf{0}\\ \mathbf{0} & \mathbf{0} & \mathbf{h}_j & \mathbf{0} & \mathbf{0}\\ \mathbf{0} & \mathbf{0} & \mathbf{0} & \ddots & \vdots\\ \mathbf{0} & \mathbf{0} & \mathbf{0} & \dots & \mathbf{h}_\alpha\end{bmatrix}, \tag{18a – b}$$

where $\mathbf{k}_j=[\mathrm{k}_{j,pq}=\mathrm{f}_p/\mathrm{x}_q]$ and $\mathbf{h}_j=[\mathrm{h}_{j,pq}=\mathrm{f}_p/\mathrm{ix}_q]$ are the unknown stiffness and damping matrices of local dimension n respectively associated with a particular joint that must be identified. The indices p and q are written in terms of the local sub-matrix indices, whereas P and Q reference the system matrix indices.

First a residual vector at the rth mode is defined as

$$\mathbf{E}_r=\{\hat{\lambda}_r^2\mathbf{M}+\hat{\lambda}_r\mathbf{C}+\mathbf{K}+\mathbf{k}+i\mathbf{h}\}\,\hat{\boldsymbol{\psi}}_r, \tag{19}$$

where $\hat{\lambda}_r$ and $\hat{\boldsymbol{\psi}}_r$ are measured values. Next, an objective function at the rth mode is defined as

$$\xi_r=\mathbf{E}_r^{*t}\mathbf{E}_r, \tag{20}$$

where superscripts $*$ and t indicate complex conjugate and transpose, respectively. To minimize this function with respect to the jth joint stiffness and damping matrices, the required conditions are

$$\frac{\partial\xi_r}{\partial k_{j,PQ}}=\frac{\partial\mathbf{E}_r^{*t}}{\partial k_{j,PQ}}\mathbf{E}_r+\mathbf{E}_r^{*t}\frac{\partial\mathbf{E}_r}{\partial k_{j,PQ}}=0 \tag{21}$$

$$\frac{\partial\xi_r}{\partial h_{j,PQ}}=\frac{\partial\mathbf{E}_r^{*t}}{\partial h_{j,PQ}}\mathbf{E}_r+\mathbf{E}_r^{*t}\frac{\partial\mathbf{E}_r}{\partial h_{j,PQ}}=0. \tag{22}$$

A mapping relationship between p and q for each joint to the P and Q of the system is required for numerical implementation of the procedure which will be unique for a specific system. Note that the proposed formulation as given by (21) and (22) differ from the prior formulation of Kim et al. [3], where only $\partial\,\xi_r/\partial\mathrm{k}_{pp}$ and $\partial\,\xi_r/\partial\mathrm{c}_{pp}$ were necessary since **c** and **k** contained only the diagonal elements. Their assumption [3] simplified the minimization criteria resulting in two equations and two unknown parameters for each joint diagonal term, $c_{j,pp}$ and $k_{j,pp}$. Conversely, a fully populated joint matrix results in $2n^2$ equations and unknowns for each joint for the method of this article. When partially differentiating Eq. (19) with respect to joint stiffness and damping terms, the following relationships are found:

$$\frac{\partial\mathbf{E}_r^{*t}}{\partial k_{j,PQ}}=\hat{\boldsymbol{\psi}}_r^{*t}\mathbf{J}_{PQ}^t \tag{23}$$

$$\frac{\partial\mathbf{E}_r}{\partial k_{j,PQ}}=\mathbf{J}_{PQ}\hat{\boldsymbol{\psi}}_r \tag{24}$$

$$\frac{\partial\mathbf{E}_r^{*t}}{\partial h_{j,PQ}}=-i\hat{\boldsymbol{\psi}}_r^{*t}\mathbf{J}_{PQ}^t \tag{25}$$

$$\frac{\partial\mathbf{E}_r}{\partial h_{j,PQ}}=i\mathbf{J}_{PQ}\hat{\boldsymbol{\psi}}_r \tag{26}$$

where $\mathbf{J}_{PQ}$ is a component isolation matrix of dimension N defined as

$$\mathbf{J}_{PQ}=\begin{vmatrix}1 & \text{at} & J_{PQ}\\ 0 & \text{else} & \end{vmatrix}. \tag{27}$$

Substituting Eqs. (23)–(26) and (19) into Eq. (20) yields

$$\frac{\partial\xi_r}{\partial k_{j,PQ}}=0=A_{r,PQ}+2\sum_{q=1}^{n}\{k_{j,Pq}\mathrm{Re}(i\hat{\psi}_{r,Q}^{*}\hat{\psi}_{r,q})+h_{j,Pq}\mathrm{Re}(i\hat{\psi}_{r,Q}^{*}\hat{\psi}_{r,q})\} \tag{28}$$

$$\frac{\partial \xi_r}{\partial h_{j,PQ}} = 0 = B_{r,PQ} + 2\sum_{q=1}^{n}\{-k_{j,Pq}\mathrm{Re}(i\hat{\psi}^*_{r,Q}\hat{\psi}_{r,q}) + h_{j,Pq}\mathrm{Re}(\psi^*_{r,Q}\hat{\psi}_{r,q})\}, \tag{29}$$

where Re is the real value operator and the known quantities are collected as

$$A_{r,PQ} = \sum_{q=1}^{n}\{M_{Pq}\mathrm{Re}(\hat{\lambda}_r^2\hat{\psi}^*_{r,Q}\hat{\psi}_{r,q}) + C_{Pq}\mathrm{Re}(\hat{\lambda}_r\hat{\psi}^*_{r,Q}\hat{\psi}_{r,q}) + K_{Pq}\mathrm{Re}(\hat{\psi}^*_{r,Q}\hat{\psi}_{r,q})\} \tag{30}$$

$$B_{r,PQ} = -2\sum_{q=1}^{n}\{M_{Pq}\mathrm{Re}(i\hat{\lambda}_r^2\hat{\psi}^*_{r,Q}\hat{\psi}_{r,q}) + C_{Pq}\mathrm{Re}(i\hat{\lambda}_r\hat{\psi}^*_{r,Q}\hat{\psi}_{r,q}) + K_{Pq}\mathrm{Re}(i\hat{\psi}^*_{r,Q}\hat{\psi}_{r,q})\}. \tag{31}$$

When two or more modes are utilized in the identification method, the assembled minimized equations of motion are solved using the pseudo-inverse process. The coefficient matrices are populated using Eqs. (28)–(31) in a least squares manner as

$$\begin{bmatrix} \begin{bmatrix}[Y_{11}] & [Y_{12}]\\ [Y_{21}] & [Y_{22}]\end{bmatrix}_1 \\ \begin{bmatrix}[Y_{11}] & [Y_{12}]\\ [Y_{21}] & [Y_{22}]\end{bmatrix}_2 \\ \vdots \\ \begin{bmatrix}[Y_{11}] & [Y_{12}]\\ [Y_{21}] & [Y_{22}]\end{bmatrix}_r \end{bmatrix} \begin{bmatrix}\mathbf{k}'\\ \mathbf{h}'\end{bmatrix}_j = \begin{bmatrix} \begin{bmatrix}\mathbf{A}'_1\\ \mathbf{B}'_1\end{bmatrix} \\ \begin{bmatrix}\mathbf{A}'_2\\ \mathbf{B}'_2\end{bmatrix} \\ \vdots \\ \begin{bmatrix}\mathbf{A}'_r\\ \mathbf{B}'_r\end{bmatrix} \end{bmatrix}, \tag{32}$$

where $\begin{bmatrix}\mathbf{k}' & \mathbf{h}'\end{bmatrix}_j^t$ and $\begin{bmatrix}\mathbf{A}' & \mathbf{B}'\end{bmatrix}^t$ denote the reassembly of matrices into column vectors. A weighting methodology is adopted that scales the coefficient matrix, **Y**, such that the greatest magnitude in a given row is unity. Here, the weighting nomenclature is introduced as

$$\mathbf{Y}_w \begin{bmatrix}\mathbf{k}'\\ \mathbf{h}'\end{bmatrix}_j = \begin{bmatrix}\mathbf{A}'\\ \mathbf{B}'\end{bmatrix}_w \tag{33}$$

$$\mathbf{Y}_w = \mathbf{W}\,\mathbf{Y} \tag{34}$$

$$\begin{bmatrix}\mathbf{A}'\\ \mathbf{B}'\end{bmatrix}_w = \mathbf{W}\begin{bmatrix}\mathbf{A}'\\ \mathbf{B}'\end{bmatrix}. \tag{35}$$

Additionally, the symmetry of the joint stiffness and damping matrices (assumed or known *a priori*) is imposed using a transformation matrix, $\mathbf{T}_s$, as

$$\begin{bmatrix}\mathbf{k}'\\ \mathbf{h}'\end{bmatrix}_j = \mathbf{T}_s\begin{bmatrix}\mathbf{k}'\\ \mathbf{h}'\end{bmatrix}_{s,j}. \tag{36}$$

When Eqs. (35) and (36) are substituted into (32), the equations for the solution of the *j*th joint can be written as

$$\begin{bmatrix}\mathbf{k}'\\ \mathbf{h}'\end{bmatrix}_j = \mathbf{T}_s[\mathbf{Y}_w\mathbf{T}_s]^+\begin{bmatrix}\mathbf{A}'\\ \mathbf{B}'\end{bmatrix}_w, \tag{37}$$

where the superscript, +, indicates the pseudo-inverse.

The above formulation requires that the eigenvector be precisely known at each joint location. However, this is not always possible in experimental studies. Therefore, when the response at the joint location cannot be measured directly, the measured eigenvector components are interpolated using the computational model to estimate the eigenvector components at the joint degrees of freedom using a modified version of Kidder's method [18]. First, several transformation matrices are defined as

$$\boldsymbol{\psi}_{r,o} = \mathbf{T}_o\boldsymbol{\psi}_r,\ \boldsymbol{\psi}_{r,\bar{o}} = \mathbf{T}_{\bar{o}}\boldsymbol{\psi}_r,\ \boldsymbol{\psi}_{r,m} = \mathbf{T}_m\boldsymbol{\psi}_r,\ \text{and}\ \boldsymbol{\psi}_{r,\bar{m}} = \mathbf{T}_{\bar{m}}\boldsymbol{\psi}_r, \tag{38a – d}$$

where $\boldsymbol{\psi}_r$ is the complete eigenvector and subsets $\boldsymbol{\psi}_{r,o}$ contain the eigenvector components at the joints, $\boldsymbol{\psi}_{r,\bar{o}}$ contains all components except at the joints, and $\boldsymbol{\psi}_{r,m}$ and $\boldsymbol{\psi}_{r,\bar{m}}$ contain measured and unmeasured components of the eigenvector, respectively. The transformation matrices are filled with 0 and 1 entries that reduce the eigenvectors to a subset of the entries. For example, a complete eigenvector, $\boldsymbol{\psi}_r$, has dimension, $N \times 1$. Given that m components of the vector are measured, the transformation matrix, $\mathbf{T}_m$, is formed of dimension $m \times N$; thus, $\boldsymbol{\psi}_{r,m} = \mathbf{T}_m\boldsymbol{\psi}_r$, where $\boldsymbol{\psi}_{r,m}$ has a dimension of $m \times 1$. Next, the dynamic stiffness (**Z**) for the system at mode r can be decomposed into that of the unconstrained structure as

$$\mathbf{Z} = \lambda_r^2\mathbf{M} + \lambda_r\mathbf{C} + \mathbf{K} \tag{39}$$

and of the joints as

$$\mathbf{z} = \mathbf{k} + i\mathbf{h}. \tag{40}$$

The eigenvalue problem for the assembled system is then formulated as

$$\{\mathbf{Z} + \mathbf{z}\}\boldsymbol{\psi}_r = \mathbf{0}. \tag{41}$$

By premultiplying Eq. (41) by $\mathbf{T}_{\overline{o}}$, the unknown joint dynamic stiffness is removed from the eigenvalue problem as

$$\mathbf{T}_{\overline{o}}\{\mathbf{Z} + \mathbf{z}\}\boldsymbol{\psi}_r = \mathbf{T}_{\overline{o}}\mathbf{Z}\boldsymbol{\psi}_r = \mathbf{0}. \tag{42}$$

Finally, the eigenvector can be decomposed into measured and unmeasured components as

$$\mathbf{T}_{\overline{o}}\mathbf{Z}\begin{bmatrix}\mathbf{T}_m^t & \mathbf{T}_{\overline{m}}^t\end{bmatrix}\begin{bmatrix}\mathbf{T}_m \\ \mathbf{T}_{\overline{m}}\end{bmatrix}\boldsymbol{\psi}_r = \mathbf{0}. \tag{43}$$

This permits the unmeasured values ($\boldsymbol{\psi}_{r,\overline{m}}$) of the eigenvector to be computed from the measured values ($\boldsymbol{\psi}_{r,m}$) as

$$\boldsymbol{\psi}_{r,\overline{m}} = -[\mathbf{T}_{\overline{o}}\mathbf{Z}\mathbf{T}_{\overline{m}}^t]^+[\mathbf{T}_{\overline{o}}\mathbf{Z}\mathbf{T}_m^t]\boldsymbol{\psi}_{r,m}. \tag{44}$$

It has been found that the interpolation of unmeasured eigenvector components using methods similar to Eq. (44) is quite accurate for lower modes and the implication is that the interpolation is dependent upon the form of the original finite element model [19]. At a minimum, the required number of measured components of the eigenvector is equal to the number of degrees of freedom of the all of the joints. Consideration of the minimum quantity, location, and the direction of the measured degrees of freedom is undertaken as described in Section 3 to aid in proper interpolation of rotational degrees of freedom from translational measurements.

6. Uniqueness and conditioning of the proposed joint identification method

Analytical minimization of the objective function in the previous section with respect to each joint at a single mode leads to a linear system of $2n^2$ equations with $2n^2$ unknowns (Eq. (32)). Thus, the problem is linear; however, issues of matrix rank and conditioning remain to be examined. To insure full rank, a set of modes must be selected for the identification method such that each term in the joint stiffness matrix interacts with one or more modes of vibration. For example, selection of the first three rigid body modes of the beam experiment insures that all terms of each joint stiffness matrix interact with at least one of the modes and full rank is accomplished. Each additional mode adds a set of $2n^2$ equations without increasing the number of unknowns and leads to an over-determined system.

A computational investigation is undertaken to examine the conditioning of the proposed identification method using the computational model of the beam experiment from Section 4. If the columns of the matrix, $\mathbf{Y_w}$, are close to being linearly related, the problem is ill-conditioned and the presence of noise in the measured vibration data could significantly influence the ability to identify the joint properties. The condition number, κ_{cond}, of the matrix, $\mathbf{Y_w}$, is defined as

$$\kappa_{\text{cond}}(\mathbf{Y}_{\text{w}}) = \frac{\sigma_{\max}(\mathbf{Y}_{\text{w}})}{\sigma_{\min}(\mathbf{Y}_{\text{w}})}, \tag{45}$$

where $\sigma_{\min}(\mathbf{Y_w})$ and $\sigma_{\max}(\mathbf{Y_w})$ are the minimum and maximum singular values of $\mathbf{Y_w}$, respectively. The condition number is plotted against the non-dimensional joint stiffness scaling parameter $\overline{k}$ in Fig. 3 for two selections of modes used in the simulated identification method. Physically, $\overline{k}$ is interpreted as the ratio between the joint stiffness to the beam flexural stiffness. For $\overline{k}=0$, the end joints of the beam approach free–free boundary conditions; conversely, when $\overline{k}\to\infty$, the end joints approach ideally pinned boundary conditions, assuming that $\overline{k}_\theta = 0$. The condition number remains between 3 and 5 as $\overline{k}$ approaches 50 where the value begins to significantly increase. By including additional modes (say r=4–6) in the identification procedure, the condition number is improved for larger values of $\overline{k}$ as shown in Fig. 3b.

Fig. 4 shows the sensitivities of the system eigenvalues as a function of $\overline{k}$, assuming that $\overline{k}_\theta = 0$ for the first six modes. Modes r=1, 2 and 3 correspond to the rigid body modes and r=4, 5 and 6 are the flexural modes. The natural frequencies (ω_r) are normalized by the first beam bending mode (ω_4) with $\overline{k}=0$ such that $\overline{\omega}_r = \omega_r/\omega_4$. The sensitivity of mode r=2 tends to flatten above $\overline{k}=10^2$. This location corresponds to the increasing value of the $\kappa_{\text{cond}}(\mathbf{Y}_{\text{w}})$ as would be expected. Considering the above analysis, the proposed methodology appears well-posed up to a limiting value of the ratio between joint transverse and beam flexure stiffness, $\overline{k}$.

7. Experimental validation of the proposed identification method

The modal testing of the freely suspended elastic beam permits a direct comparison of the theoretical and experimental eigensolutions as well as the extraction of $\mathbf{C}$ assuming proportional damping of the steel beam. The measured natural frequencies for the first three elastic deformation modes (r=4–6) are listed in Table 1. The Timoshenko beam theory captures each mode within 1–2 Hz (percent difference between 0.2% and 0.6%), whereas the Euler theory is still reasonably accurate (within 10 Hz and a percent difference of 1.1%) at the third elastic mode (r=6).

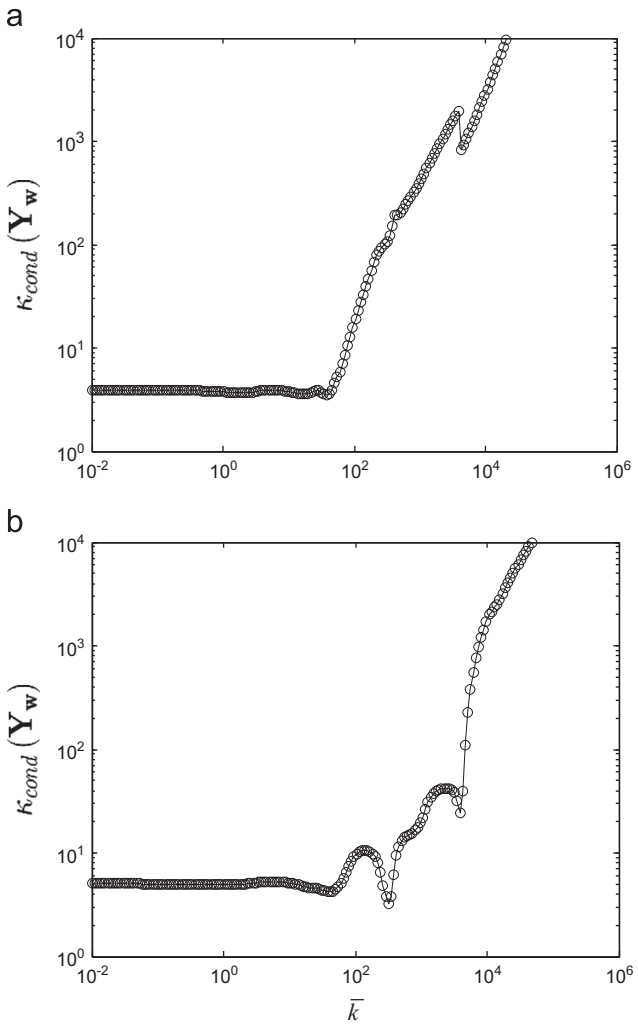

Fig. 3. Condition number of simulated identification method as a function of dimensionless joint stiffness$\bar{k}$. Key: (a) Modes $r=1$, 2, and 3 used in identification method and (b) modes $r=1$, 2, 3, 4, 5, and 6 used in identification method.

The end-supported inverse beam experiment exhibits nearly repeated roots with a separation of 2 Hz over a frequency range of interest of up to 1024 Hz, in which six modes of vibration are captured. A statistical analysis of the observations $\Gamma_o = [\mathbf{A}' \quad \mathbf{B}']_w^t$, curve-fitted values $\Gamma_c = \mathbf{Y}_w[\mathbf{k}' \quad \mathbf{h}']_j^t$, and residuals $\Gamma_\varepsilon = \Gamma_o - \Gamma_c$ is performed to establish a confidence interval for the identified stiffness matrix. The reader is referred to Draper and Smith [20] for a detailed description of the statistical terms. Fig. 5 shows the plot of Γ_o against Γ_c values, and an agreement is achieved through the full range with a coefficient of multiple determination of 0.99. The variance and covariance terms are contained in the diagonal and off-diagonal elements of $(\mathbf{Y}_w^t\mathbf{Y}_w)^{-1}\sigma^2$, respectively, where σ^2 is estimated by the mean square error of the residuals, s^2. Assuming a normal distribution and a confidence level of 95%, the identified normalized **k** elements are shown in Table 2. The dominant terms of k_{11}, k_{22}, k_{12}, and k_{21} exhibit a range that is within $\pm 3\%$ to 9% with the greatest range existing at joint I for k_{11} direction with a range of $\pm 9\%$. The range of values within the confidence interval for stiffness terms k_{13}, k_{31}, k_{32}, k_{23}, and k_{33} pass through zero. These terms are difficult to distinguish from zero; nevertheless, their presence is still required to obtain adequate results. The terms k_{13}, k_{31}, k_{32}, and k_{23} were intentionally canceled with opposing cylinders at each joint; however, misalignments in the transverse direction or non-symmetric vertical placement can introduce stiffness coupling for these directions. The structural loss factor matrix elements ($\gamma_{ij} = h_{ij}/k_{ij}$) are shown in Table 3 within in a 95% confidence interval for each joint. Since, the k_{13}, k_{31}, k_{32}, k_{23}, and k_{33} terms are near zero, division of the structural damping components by these terms yields physically meaningless results and are not shown in Table 3.

The identified joint dynamic stiffness matrices are employed to forward predict the modal parameters and frequency response functions. Table 4 lists the natural frequencies and the forward predictions which agree within 3% with the highest error occurring at a rigid body mode ($r=2$). The corresponding eigenvectors are plotted in Fig. 6. Although not used in the identification process, all of the measured eigenvector components are plotted against the forward prediction.

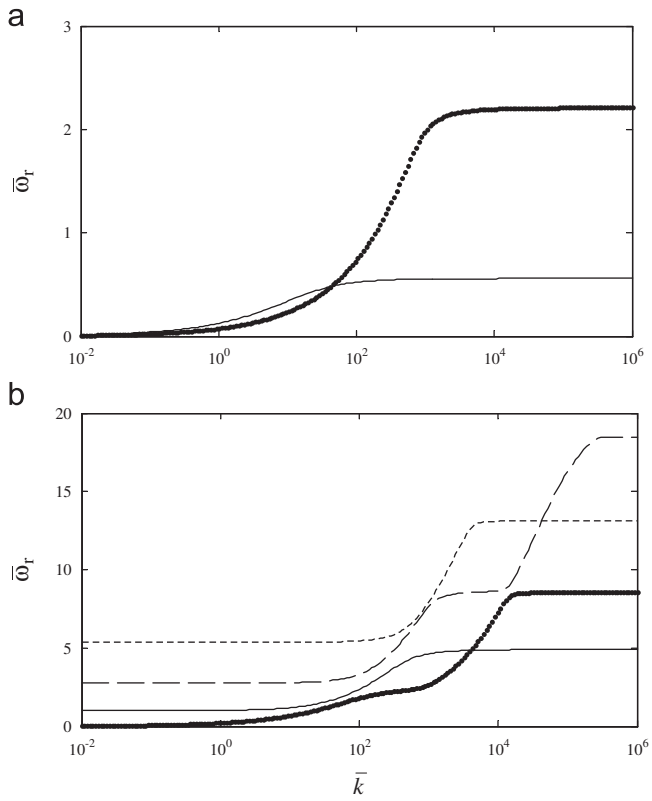

Fig. 4. Sensitivity of the eigenvalues as a function of dimensionless joint stiffness$\bar{k}$. Key: (a) ●●●● $r=1$; — $r=2$ and (b) ●●●● $r=3$; — $r=4$; – – $r=5$; - - - $r=6$.

Table 1
Comparison of first three natural frequencies for the unsupported elastic beam (under free–free boundary conditions).

Mode index r	Experiment $\omega_r/2\pi$ (Hz)	Theory (Timoshenko) $\omega_r/2\pi$ (Hz)	Theory (Euler) $\omega_r/2\pi$ (Hz)
4	161 ($\zeta_1=0.4\%$)*	160	160
5	441 ($\zeta_2=0.1\%$)*	439	442
6	858 ($\zeta_3=0.1\%$)*	856	868

* Modal damping ratio.

Forward predictions of the accelerance spectra $\tilde{\mathbf{A}}(\omega)$ are computed by a direct inversion of the assembled dynamic stiffness matrices as

$$\tilde{\mathbf{A}}(\omega) = -\omega^2(\mathbf{Z}(\omega)+\mathbf{z})^{-1}\mathbf{f}(\omega). \tag{46}$$

The driving point comparison Fig. 7 exhibits good agreement, though some regions show discrepancies. This may suggest a deficiency in a simple (assumed) structural damping model. Similar results are observed for the transverse cross-point accelerance shown in Fig. 8. The cross point spectrum between transverse and longitudinal motions in Fig. 9 exhibits influence from out-of-plane bending vibrations at 330 and 855 Hz. It is observed during measurements that impact location errors at the end of the beam excite these lightly damped structural modes; whereas the transverse impacts are less sensitive to this issue. Both cross-point comparisons show that the forward prediction and measurement were out of phase near the antiresonance at 440 Hz, which can be explained by a poor signal to noise ratio in this frequency range.

8. Uniaxial joint characterization using the direct method

8.1. Comparison of direct and inverse tests

The direct component test employs a uniaxial hydraulically actuated, close loop servo-controlled elastomer test machine. Typically a sinusoidal displacement, $x(t)$, is applied to the top side of the specimen, and the transmitted force, $f(t)$,

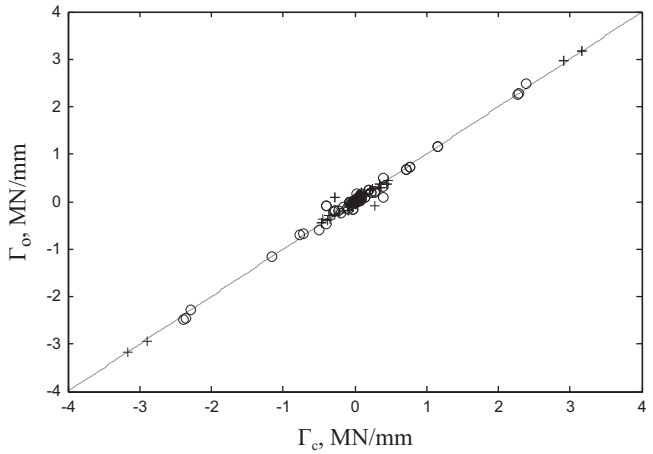

Fig. 5. Observed data, $\Gamma_o = [\mathbf{A}' \quad \mathbf{B}']_w^t$, against the curve-fitted data, $\Gamma_c = \mathbf{Y}_w[\mathbf{k}' \quad \mathbf{h}']_j^t$; Key: + joint 1; ○ joint 2; - - - linear fit with slope of unity without a zero offset.

Table 2
Identified normalized dynamic stiffness matrix elements within a 95% confidence interval from the resonant beam experiment.

Joint I			Joint II		
k_{11}=[129,153]	k_{12}=[97,109]	k_{13} =[2,8]	k_{11}=[170,180]	k_{12}=[−115,–123]	k_{13}=[7,11]
k_{21}=[97,109]	k_{22}=[124,135]	k_{23}=[−2.1,1.9]	k_{21}=[−115,–123]	k_{22}=[165,175]	k_{23}=[−5,−1]
k_{31}=[−28,10]	k_{32}=[−10, 4]	k_{33}=[−2,4]	k_{31}=[−6,8]	k_{32}=[−5,9]	k_{33}=[−2.9,3.1]

Table 3
Identified loss factor matrix elements within a 95% confidence interval from the resonant beam experiment.

Joint 1			Joint 2		
γ_{11}=[0.02,0.2]	γ_{12}=[0.01,0.13]	–	γ_{11}=[0.09,0.15]	γ_{12}=[0.12,0.20]	–
γ_{21}=[0.01,0.13]	γ_{22}=[0,0.07]	–	γ_{21}=[0.12,0.20]	γ_{22}=[0.13,0.19]	–
–	–	–	–	–	–

Table 4
Comparison of natural frequencies for supported resonant beam experiment.

Mode index r	Experiment $\omega_r/2\pi$ (Hz)	Theory (Timoshenko) $\omega_r/2\pi$ (Hz)	Theory (Euler) $\omega_r/2\pi$ (Hz)
1	77.4	79.0	76.7
2	79.5	82.4	82.8
3	204	202	202
4	266	265	266
5	469	474	476
6	865	870	879

at the bottom of the specimen is measured at the same frequency. The dynamic stiffness can be defined as

$$\tilde{k}_d(\omega) = \frac{f}{x} e^{i\delta} = |\tilde{k}_d| \angle \delta = k + ih, \tag{47}$$

where δ is the loss angle. The loss factor, $\gamma = \tan\delta$, is defined as

$$\tilde{k}_d(\omega) = k(1 + i\gamma). \tag{48}$$

The elastomeric cylinders are characterized in three different configurations: (1) compression, (2) shear, and (3) angled as depicted in Fig. 10. The compression configuration consists of a single cylinder. The shear and angled configurations are conducted with a pair of elastomeric cylinders to ensure appropriate boundary conditions. The diameter and height of each cylinder is 25.4 mm. Metallic caps are bonded to both sides of each cylinder to prevent damage to the elastomer

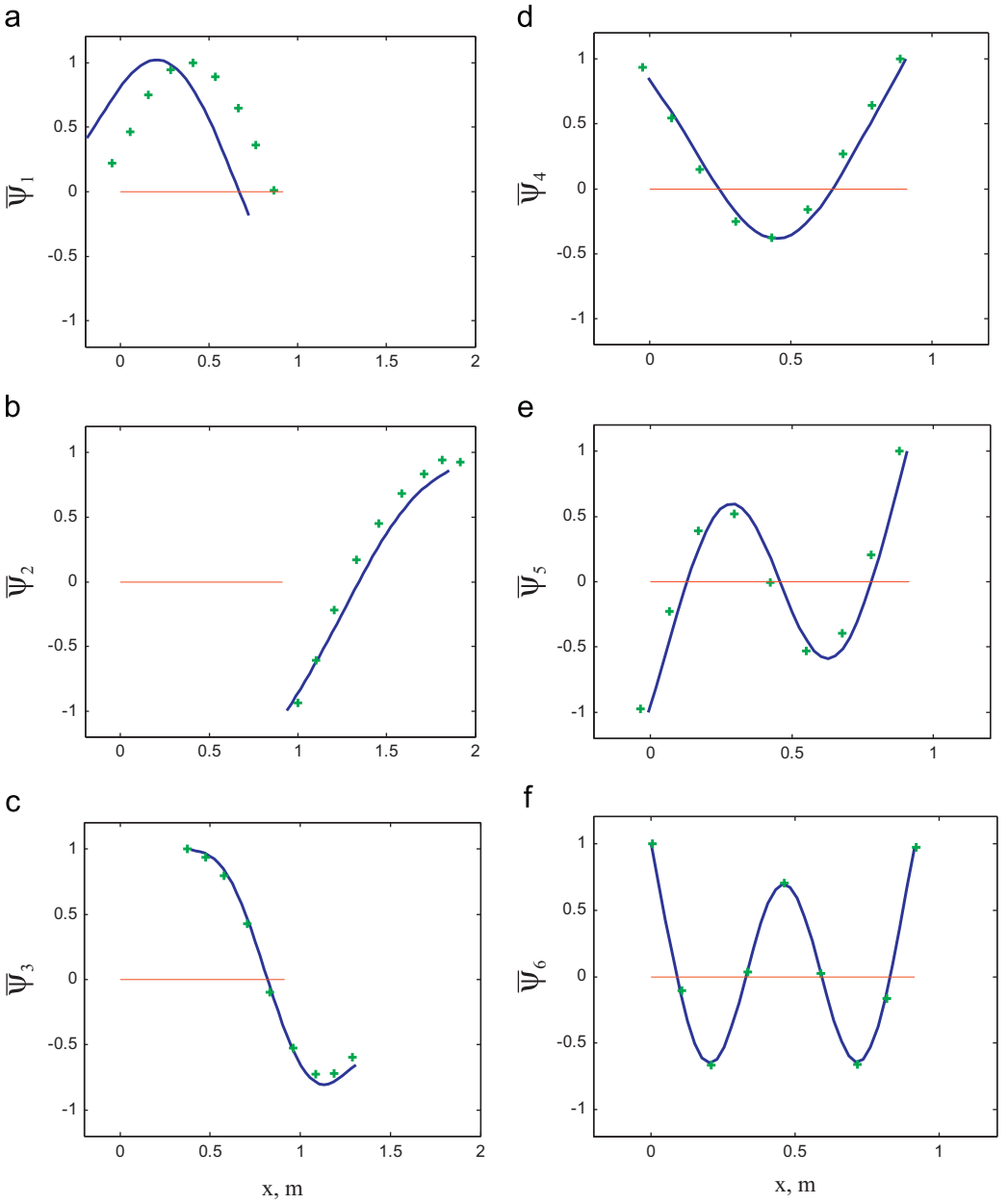

Fig. 6. Eigenvectors of the resonant beam experiment at (a) $r=1$, (b) $r=2$, (c) $r=3$, (d) $r=4$, (e) $r=5$ and (f) $r=6$. Key: + measured using modal measurements; —— theory with identified dynamic stiffness supports.

during disassembly. The direct measurements correspond with specific linear combinations of the elements of the cylinder stiffness matrix of Eq. (8) as: 1. shear=2a, 2. compression=b, and 3. angled=a+b.

The dynamic characterization is conducted at an initial preset of 0.5 mm from 5 to 200 Hz at 5 Hz increments. Under each configuration, the peak-to-peak amplitude is specified at 0.1 mm, 0.05 mm, or 0.01 mm. Dynamic testing at the lowest amplitude (0.01 mm peak-to-peak) appears to be at or near the limit of the test machine's capability.

8.2. Results and discussion

The dynamic stiffness spectra of elastomeric cylinders exhibit considerable amplitude and frequency dependence in the direct tests as shown in Fig. 11. The highest sensitivity to frequency dependence is observed below 50 Hz. The measured $|\tilde{k}_d|$ increases for each configuration as the amplitude of the excitation decreased by a factor of 2.1, 1.5, and 2.0 for the compression, shear, and the angled configurations, respectively. The loss factor is nearly constant with respect to

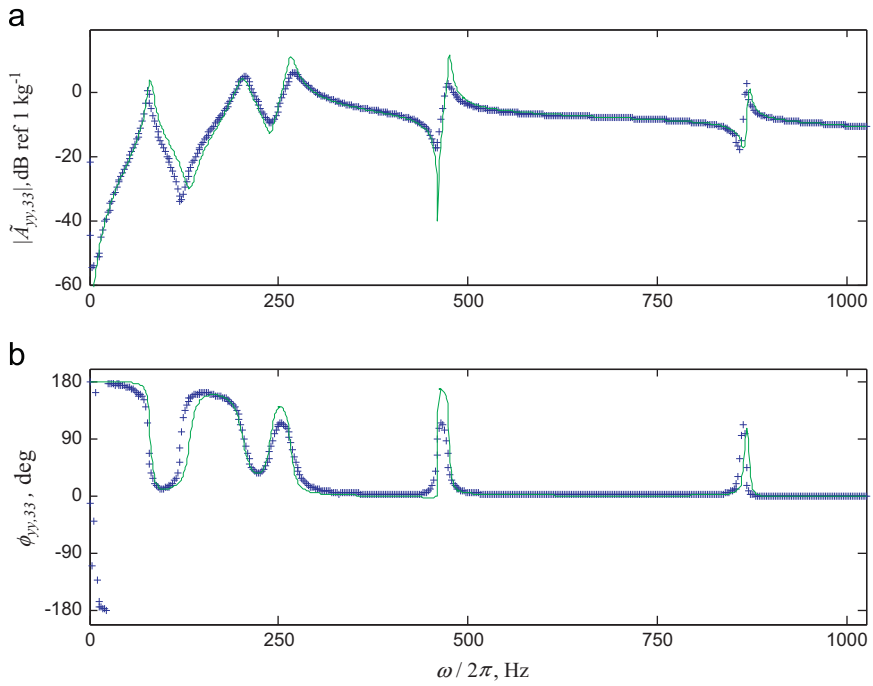

Fig. 7. Driving point accelerance for the resonant beam experiment in the transverse direction at point 3. (a) magnitude and (b) phase. Key: (—) predicted using Eq. (46); (+) measured.

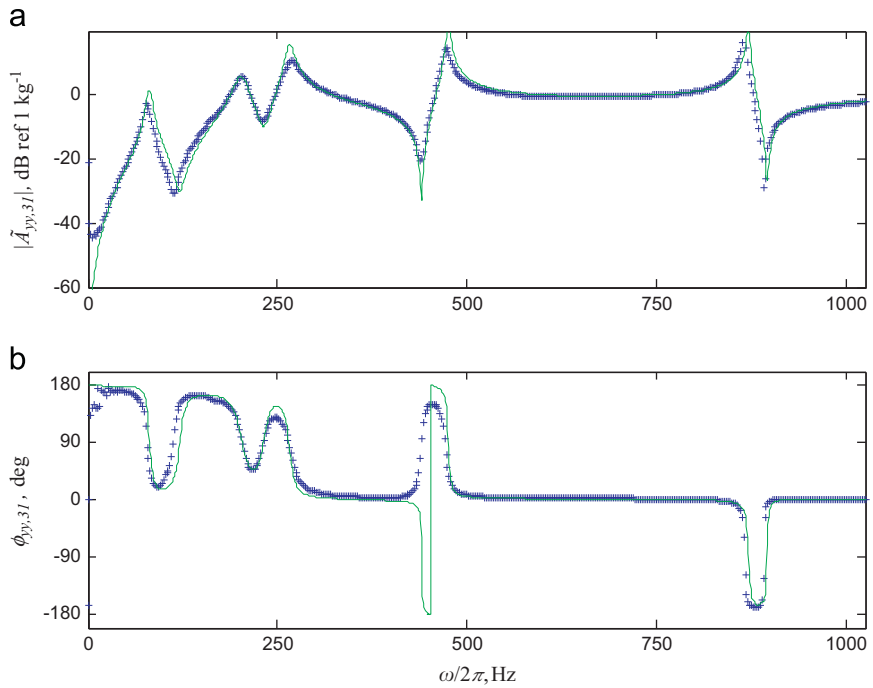

Fig. 8. Cross point accelerance for the resonant beam experiment with a transverse force input at point 1 and transverse response at point 3 (a) magnitude and (b) phase. Key: (—) predicted using Eq. (46); (+) measured.

frequency; however, it decreases by half when the peak-to-peak amplitude of the excitation is reduced from 0.1 mm to 0.01. These results confirm that a linearized dynamic joint stiffness matrix is consistent with a structural damping model at very small operating amplitudes, especially above 50 Hz. Note that the direct tests has been limited to the frequency range of 5–200 Hz; whereas, the inverse beam test extends up to 1000 Hz. For the combination of beam and joint stiffness,

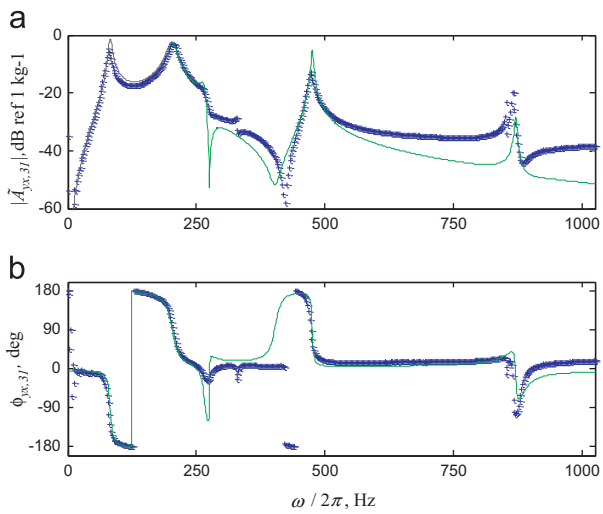

Fig. 9. Cross point accelerance for the resonant beam experiment with a longitudinal force input at point 1 and transverse response at point 3 (a) magnitude and (b) phase. Key: (—) predicted using Eq. (46); (+) measured.

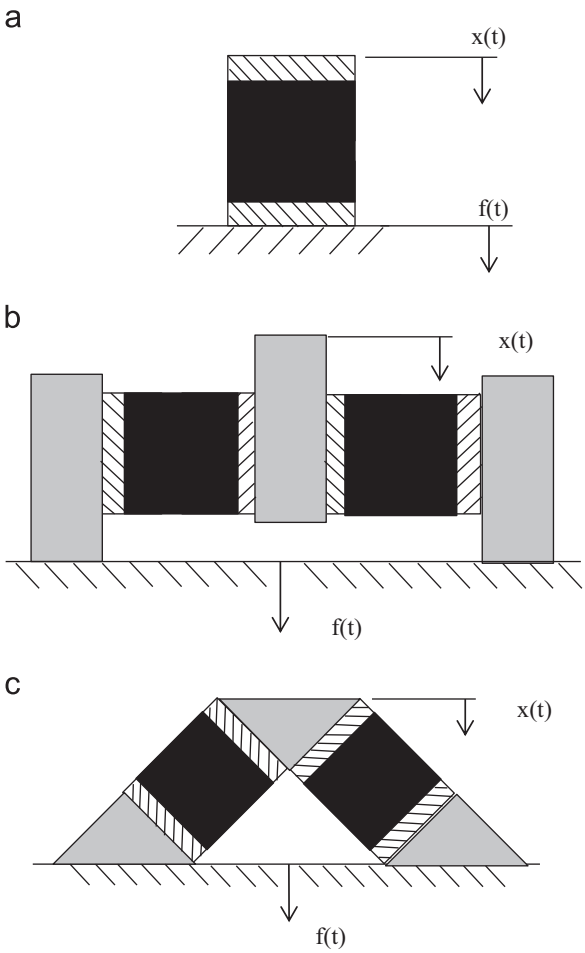

Fig. 10. Configurations used to characterize elastomeric cylinders in a non-resonant elastomer test system, (a) in compression, (b) in shear and (c) inclined at 45°. Key: elastomeric cylinders ▬; metal cap ▨; aluminum block ▭.

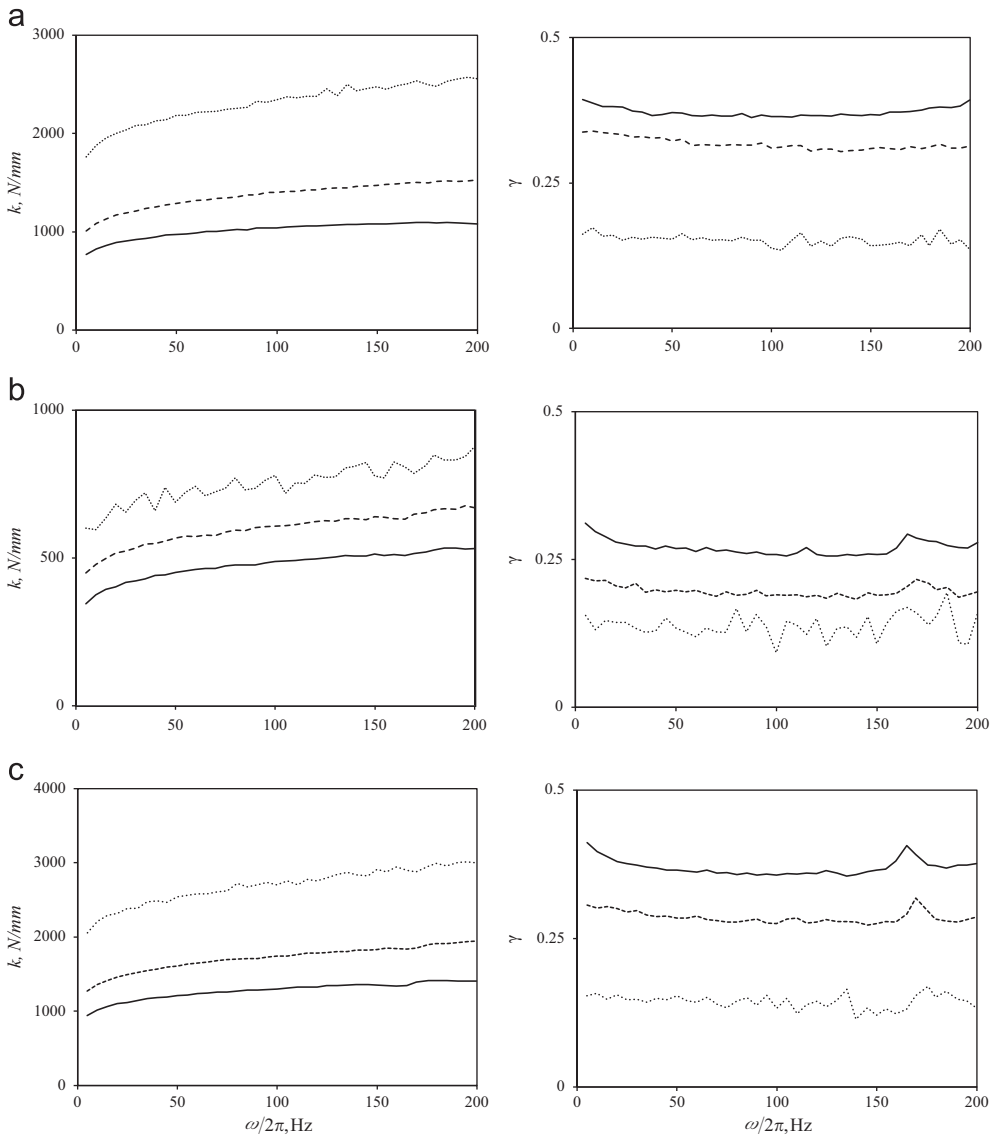

Fig. 11. Elastomeric joint characterization using non-resonant test method showing stiffness and loss factor for configurations (a) compression, (b) shear and (c) inclined at 45° as shown in Fig. 10 Key: Peak-to-peak amplitudes of, —, 0.1 mm; – – –, 0.05 mm; ……. 0.01 mm.

modes $r=5$ and 6 (beyond 400 Hz) exhibits low modal damping whereas the modal damping of modes $r=1$–4 (77–266 Hz) is significantly higher. To examine the interactions between the elastomer and a beam structure, alternate combinations of beam and joint stiffnesses could be examined. The inverse test has been limited with only impact hammer excitations and thus a linear response is expected. To observe the amplitude-dependent properties of the elastomers in the inverse test, sinusoidal excitation with higher amplitude (e.g. shaker excitation) would be needed.

Since the elastomer test machine permits only uniaxial measurements, the specimens are oriented in several configurations to measure relevant diagonal elements of the dynamic stiffness matrices. Using Eq. (13), $|\tilde{k}_d|$ is replotted in Fig. 12 showing the angled measurement in Fig. 11c against the computed value using the measured data from the shear and compression measurements shown in Fig. 11a and b, respectively. This comparison demonstrates that superposition holds near the operating points. Since there is such a strong agreement, it is expected that the computed values for the kinematic coupling terms between longitudinal and transverse directions can be similarly estimated by using Eq. (15). A comparison between the direct component and inverse system tests is now possible for k_{11}, k_{22}, k_{12} and k_{21} of the joint stiffness matrices. Since k_{13}, k_{31}, k_{32}, and k_{23} are intended to be zero, only k_{33}remains without a reference value for comparison.

Fig. 13 compares the direct dynamic stiffness and the bounded stiffness identified from the inverse test. Generally, there is good agreement between the inverse and the direct measurement at 0.01 mm peak-to-peak excitation amplitude. Fig. 14 shows the comparison between the direct loss factor and bounded loss factor from the inverse beam experiment.

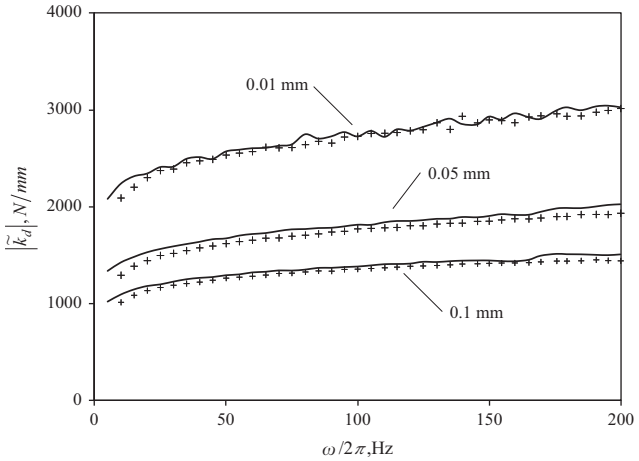

Fig. 12. Comparison of the dynamic stiffness of two elastomeric cylinders angled at 45° at three different excitation amplitudes, 0.01 mm, 0.05 mm, and 0.1 mm. Key: + computed with Eq. (15) using compression and shear measurements; — measured angled elastomeric cylinders.

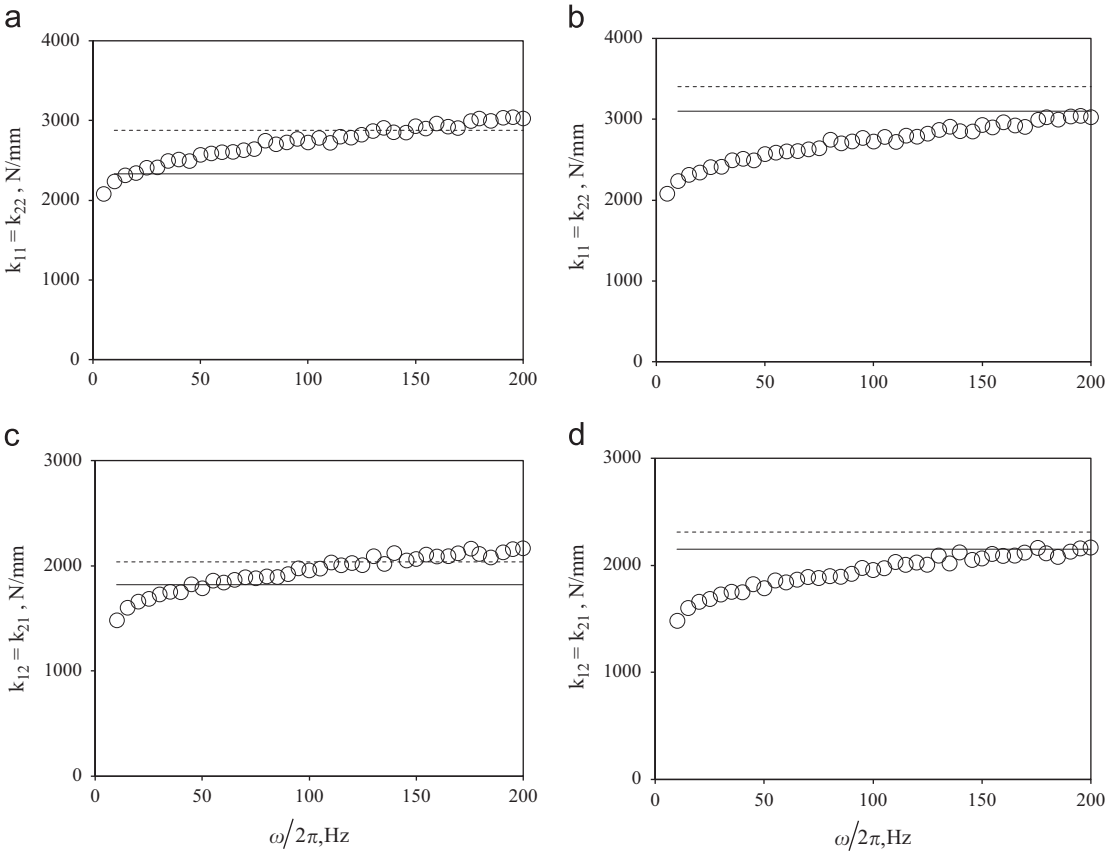

Fig. 13. Comparison of the identified stiffness from the resonant beam experiment (within 95% confidence limits) and non-resonant measurements. (a) element $k_{11}=k_{22}$ for joint I, (b) element $k_{11}=k_{22}$ for joint II, (c) element $k_{12}=k_{21}$ for joint I, (d) element $k_{12}=k_{21}$ for joint II. Key: – – – upper bound, — lower bound, and ○ direct measurement with peak-to-peak amplitude of 0.01 mm.

The average loss factor for both joints for the dominant terms is about 0.11. This value provides a lower limit to the directly measured loss factors. Overall, there is satisfactory agreement between the direct and inverse tests at joint II as seen in Fig. 14b in the small amplitude range, though the loss factor identified at joint I exhibits a wider range for the confidence interval.

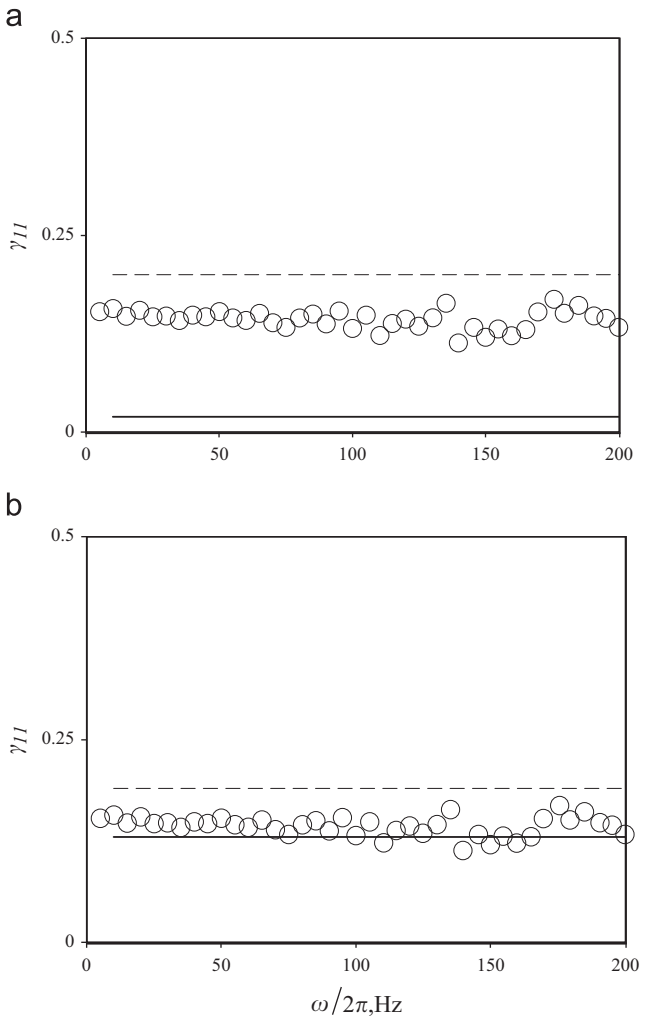

Fig. 14. Comparison of the identified loss factor from the inverse beam experiment (within 95% confidence limits) and direct measurements. (a) joint I and (b) joint II. Key: Direct measurement with peak to peak amplitude of, □, 0.05 mm; ○, 0.01; identified loss factor – – – upper bound; — lower bound;

9. Conclusion

This article has contributed to the state of the art by designing new experiments and methods that permit a direct comparison of inverse and direct methods and by extending a prior method [3] to include the identification of non-diagonal terms in the stiffness matrices of joints. The proposed methodology is employed to identify the dynamic stiffness properties of joints with dimension 3 in the inverse experiment consisting of an elastic beam with two elastomeric supporting elements. A forward model successfully predicts the measured modal parameters and accelerance spectra. Agreement is found for dynamic stiffness and loss factors between the inverse and direct methods in the small amplitude range.

There are several potential sources of error that can account for some deviations between the experimental and theoretical results. Modeling error introduced through the discretization of the beam is minimized by including rotary inertia and shear deformation into the beam theory. It is assumed the joint can be represented as lumped stiffness at a single point for a joint, even though the actual cylinder is distributed over an area. The end-supported beam experiment exhibits nearly repeated roots for the first two rigid body modes. This result increases the level of difficulty for the modal parameters to be accurately estimated for such modes of vibration. The construction of the inverse experiment itself in terms of misalignments in the cylinders in either longitudinal or angular placement can introduce coupling for the terms k_{13}, k_{31}, k_{32}, and k_{23}. Also, any non-uniformity in properties as well as differences due to machining tolerance in the overall cylinder length could lead to coupling terms in k_{13}, k_{31}, k_{32}, and k_{23}. Finally, the linearized joint properties are assumed, and therefore any nonlinearities associated with the elastomer should affect the results.

The methods in this article are not limited to metal beam and elastomeric joint systems, but rather are applicable to a more general class of jointed assemblies. The proposed identification method is well-conditioned for joint dominated

assemblies up to a limit of the stiffness ratio (between the joint and structure). Additional regularization techniques may be employed to address ill-conditioning issues above the limiting stiffness ratio. The inverse test in this article is limited to an examination of the linearized joint properties; however, the design lends itself well to incorporate different excitation levels to examine the amplitude-dependent properties of elastomers. Further, with two opposing joints, preload or displacement can be easily added without altering the system. Finally, the work has been limited to a single structure connected to ground, whereas many real-world assemblies contain two or more substructures. Despite these limitations, this article provides valuable insights for interpreting directly measured component test data with system inverse data even when the selected elastomer exhibits strong amplitude dependent properties.

Acknowledgment

We acknowledge the member organizations such as Transportation Research Center Inc., Honda R&D Americas, Inc., YUSA Corporation and F. tech of the Smart Vehicle Concepts Center (www.SmartVehicleCenter.org) and the National Science Foundation Industry/University Cooperative Research Centers program (www.nsf.gov/eng/iip/iucrc) for supporting this work.

References

[1] K.T. Yang, Y.S. Park, Joint structural parameter identification using a subset of frequency response function measurements, Mech. Syst. Signal Process 7 (6) (1993) 509–530.
[2] S. Hong, C. Lee, Identification of linearised joint structural parameters by combined use of measured and computed frequency responses, Mech. Syst. Signal Process 5 (1991) 267–277.
[3] T.R. Kim, K.F. Ehmann, S.M. Wu, Identification of joint structural parameters between substructures, J. Eng. Indust. 113 (1991) 419–424.
[4] S.W. Hong, D.M. Shamine, Y.C. Shin, An in-situ identification method for joint parameters in mechanical structures, J. Vib. Acoust. 121 (1999) 363–372.
[5] M.J. Ratcliffe, N.A.J. Lieven., A generic element-based method for joint identification, Mech. Syst. Signal Process. 14 (1) (2000) 3–28.
[6] J.S. Tsai, Y.F. Chou, The identification of dynamic characteristics of a single bolt joint, J. Sound Vib. 125 (3) (1988) 487–502.
[7] J.H. Wang, C.M. Liou, Experimental identification of mechanical joint parameters, J. Vib.Acoust. 113 (1) (1991) 28–36.
[8] J.H. Wang, C.M. Liou, Identification of parameters of structural joints by use of noise-contaminated FRFs, J. Sound Vib. 142 (2) (1990) 261–277.
[9] Y. Ren, C. Beards, Identification of joint properties of a structure using FRF data, J. Sound Vib. 186 (1995) 567–587.
[10] P. Mehta, R. Singh, Estimation of dynamic stiffness matrix of welded or glued joints using a laboratory fixture, SAE Trans. J. Passenger Cars: Mech. Sys. 112 (6) (2003) 2227–2237. 2003-01-1710.
[11] P. Mehta, R. Singh, Effect of Welded or Glued Joints on Modal Properties of an Assembly, SAE Trans. J. Passenger Cars: Mech. Sys. 112 (6) (2003) 2256–2269. 2003-01-1717.
[12] C. Lewitzke, P. Lee, Application of elastomeric components for noise and vibration isolation in the automotive industry, SAE Paper 2001-01-1447 (2001).
[13] H.J. Kim, K.J. Kim, Effects of rotational stiffness of bushings on natural frequency estimation for vehicles by substructure coupling based on frequency response functions, Int. J. Vehicle Noise Vib. 6 (2010) 215–229.
[14] S. Kim, R. Singh, Multi-dimensional characterization of vibration isolators over a wide range of frequencies, J. Sound Vib. 245 (2001) 877–913.
[15] R.D. Cook, D.S. Malkus, M.E. Plesha, Concepts and Applications of Finite Element Analysis, Third edition, John Wiley & Sons, New York, 1989.
[16] B. Peeters, H. Van der Auweraer, P. Guillaume, J. Leuridan, The PolyMAX frequency-domain method: a new standard for modal parameter estimation? Shock Vib. 11 (2004) 395–409.
[17] Z. Friedman, J. Kosmatka, An improved two-node Timoshenko beam finite element, Comp. Struct. 47 (1993) 473–481.
[18] R.L. Kidder, Reduction of structural frequency equations, AIAA J. 11 (1973) 892. 892.
[19] N.M.M. Maia, J.M.M. Silva, Experimental Modal Analysis, Research Studies Press Ltd., England, 1997.
[20] N.R. Draper, H. Smith, Applied Regression Analysis, second ed. John Wiley & Sons, Inc., New York, 1981.